

Free Energy Predictions of Ligand Binding to an α -Helix Using Steered Molecular Dynamics and Umbrella Sampling Simulations

Jan K. Marzinek,^{†,‡,§,||} Peter J. Bond,^{†,‡,⊥} Guoping Lian,^{*,§,○} Yanyan Zhao,[#] Lujia Han,[#] Massimo G. Noro,[▽] Efstratios N. Pistikopoulos,^{||} and Athanasios Mantalaris^{*,||}

[†]National University of Singapore, Department of Biological Sciences, 14 Science Drive 4, Singapore 117543

[‡]Bioinformatics Institute (A*STAR), 30 Biopolis Str., #07-01 Matrix, Singapore 138671

[§]Unilever R&D, Colworth Science Park, Sharnbrook, Bedfordshire MK44 1LQ, United Kingdom

^{||}Department of Chemical Engineering and Chemical Technology, Imperial College London, London, SW7 2BY, United Kingdom

[⊥]The Unilever Centre for Molecular Science Informatics, Department of Chemistry, University of Cambridge, Lensfield Road, Cambridge CB2 1EW, United Kingdom

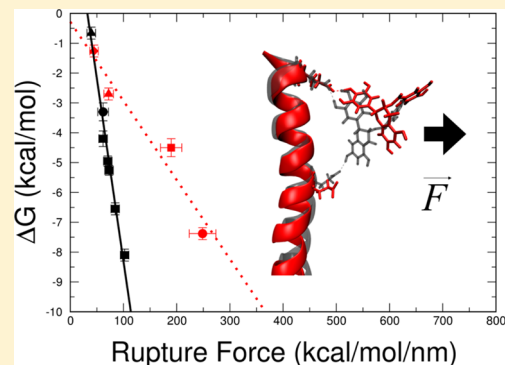
[#]China Agricultural University, Beijing 100083, People's Republic of China

[▽]Physical and Chemical Insights Group, Unilever R&D, Port Sunlight, Wirral, CH63 3JW, United Kingdom

[○]Department of Chemical and Process Engineering, University of Surrey, Guildford, Surrey GU2 7XH, United Kingdom

Supporting Information

ABSTRACT: Free energy prediction of ligand binding to macromolecules using explicit solvent molecular dynamics (MD) simulations is computationally very expensive. Recently, we reported a linear correlation between the binding free energy obtained via umbrella sampling (US) versus the rupture force from steered molecular dynamics (SMD) simulations for epigallocatechin-3-gallate (EGCG) binding to α -helical-rich keratin. This linear correlation suggests a potential route for fast free energy predictions using SMD alone. In this work, the generality of the linear correlation is further tested for several ligands interacting with the α -helical motif of keratin. These molecules have significantly varying properties, i.e., octanol/water partition coefficient ($\log P$), and/or overall charges (oleic acid, catechin, Fe^{2+} , citric acid, hydrogen citrate, dihydrogen citrate, and citrate). Using the constant loading rate of our previous study of the keratin-EGCG system, we observe that the linear correlation for keratin-EGCG can be extended to other uncharged molecules where interactions are governed by hydrogen bonds and/or a combination of hydrogen bonds and hydrophobic forces. For molecules where interactions with the keratin helix are governed primarily by electrostatics between charged molecules, a second, alternative linear correlation model is derived. While further investigations are needed to expand the molecular space and build a fully predictive model, the current approach represents a promising methodology for fast free energy predictions based on short SMD simulations (requiring picoseconds to nanoseconds of sampling) for defined biomolecular systems.



INTRODUCTION

The propensity of small molecule binding to macromolecules regulates their bioavailability and subcellular disposition. The binding free energy is also an important thermodynamic property that may be predicted in computational modeling of biological systems.^{1,2} Recently, there have been an increasing number of studies that have attempted to predict the binding free energy of small molecules to proteins via molecular dynamics (MD) simulations, often in combination with experimental measurements.^{3–5} MD-based methods for estimating binding free energies include molecular mechanics/Poisson–Boltzmann surface area (MM/PBSA),^{6,7} free energy perturbation (FEP),¹ linear interaction energy (LIE),⁸ metadynamics,⁹ replica exchange umbrella sampling (REUS),¹⁰ or umbrella sampling (US).^{11,12} Although the most predictive

methods tend to use explicit solvent and can provide accurate prediction of binding affinities,^{13–19} they are often computationally expensive. For instance, to yield well-converged properties from US calculations, sampling over time scales ranging from hundreds of nanoseconds to microseconds is often required. With the US approach, additional potentials (e.g., harmonic) provide extensive sampling along a defined reaction coordinate (e.g., distance), and multiple overlapping simulations enable estimation of the potential of mean force (PMF) and, hence, binding free energy. In addition, steered molecular dynamics (SMD) simulations are able to provide information about mechanical properties as well as structural

Received: March 14, 2014

changes within proteins, or in protein–protein and protein–ligand complexes.^{20–23} SMD has been widely used and the results are often able to reproduce results from experimental data obtained via atomic force microscopy (AFM). In SMD, a constant force or velocity is applied to a specified group of atoms attached to a “virtual spring”. SMD has also been shown to be useful as a predictive tool in drug design²⁴ by providing binding affinity estimates using the Jarzynski equality.²⁵

Recently, we reported a linear dependency between the maximum pulling force obtained from SMD simulations and the free energies obtained via US, for epigallocatechin-3-gallate (EGCG) interacting with keratin (helical segments).¹⁶ Previously, Mai et al.^{26,27} proposed a similar linear correlation for ligands binding to swine influenza A/H1N1 virus between the average rupture force (maximum pulling force) at constant loading rate (spring constant times pulling velocity), over 4 SMD trajectories, and the experimentally confirmed and MM/PBSA-based binding free energies. These findings, and the fact that the α -helix is the most prevalent protein secondary structure²⁸ accounting for 30% of the average globular protein,²⁹ motivated us to test and extend the keratin-EGCG linear dependency for other ligands. For this purpose, 7 small molecules with varying octanol/water partition coefficient ($\log P$) or protonation states binding to helical keratin segment were tested. These included oleic acid, catechin, the previously studied ferrous ion,¹⁹ and citric acid (hydrogen citrate, dihydrogen citrate, citrate).

Initially, α -helix-ligand complexes were generated by running self-assembly MD simulations and the type of interaction governing the binding process was assessed. Subsequently, the most stable conformation from each ligand-protein system was chosen, by assessing favorable protein–ligand buried surface area as well as average numbers of hydrogen bonds. We then applied SMD simulations at a velocity of 10 nm ns⁻¹ with a range of spring constants to pull each small molecule (independently 10 times) away from the α -helical segment, yielding an arithmetic average of the maximum pulling force. In this manner, for each molecule the correlation between the applied spring constant (at constant velocity) and the rupture force was obtained. Previous theoretical studies using the Bell model³⁰ have shown that the loading rate exhibits an exponential relationship with the rupture force.^{31–34} However, we observed that, for the higher velocities used in SMD simulations compared to experiment, a power function, rather than an exponential one, fit the data slightly more accurately. Subsequently and independently, the US method was used to calculate the free energy for each molecule, and a good agreement with the existing experimental data was shown. Finally, we plotted the rupture force for each molecule at the loading rate used in the previous keratin–EGCG study¹⁶ against the calculated free energies. Not all molecules studied herein with ranging physicochemical properties followed the linear correlation that we observed in a previous study.¹⁶ The linear correlation observed for keratin–EGCG could be only extended to molecules with a total charge of zero where the interaction is governed by hydrogen bonds (citric acid) and/or a combination of hydrogen bonds and hydrophobic interactions (catechin). For molecules where interactions are primarily governed by electrostatics between charged molecules (dihydrogen citrate, hydrogen citrate, citrate, and the previously studied ferrous ion¹⁹), a second (different) linear correlation is observed. Oleic acid with its carboxylate group treated in the protonated form did not follow either of the two linear

correlations, because of a dominantly hydrophobic interaction with keratin. It is likely that a similar strategy would enable the generation of linear correlations for closely related molecular series dominated by hydrophobic forces, although further investigations are needed to expand the molecular space for such molecules. Here, we limited our study to molecules interacting with the simplest and most prevalent secondary structural motif of a stable α -helix that does not undergo any secondary structural changes. Additional implementation and assessment will likely be required for more-complex proteins, and/or where significant conformational changes upon ligand binding occur. Clearly, more studies are needed to extend the method to other biomolecules and ligand systems. Nevertheless, our approach represents a promising methodology for fast free energy predictions based on short SMD simulations (requiring picoseconds to nanoseconds of sampling) in comparison with rigorous free energy methods (typically requiring nanosecond to microsecond time scale sampling), which may be tested in the future in expanded chemical space.

METHODOLOGY

Computational Details. The ligand molecules studied herein are listed in Table 1 and their molecular structures are

Table 1. (A) Small Molecules Evaluated in This Study with Varying Octanol/Water ($\log P$) Partition Coefficient, and (B) Charged Species Evaluated in This Study^a

(A) Small Molecules Evaluated in This Study				
molecule name	CAS number	$\log P$	ref	molecular weight [Da]
oleic acid	112-80-1	7.64	35	282
epigallocatechin-3-gallate	989-51-5	2.08	36	458
catechin	154-23-4	0.51	37	290
citric acid	72-92-9	-1.721	38	192
(B) Charged Species Evaluated in This Study				
molecule name	overall charge	pH range	molecular weight [Da]	
dihydrogen citrate	-1	3.29–4.77	191	
hydrogen citrate	-2	4.77–6.39	190	
citrate	-3	>6.39	189	
Fe ²⁺	+2	N/A ^b	58	

^aDifferent protonation states (depending on the pH range) of citric acid as well as ferrous ion are given. Citric acid pK_a values: $pK_{a1} = 3.29$, $pK_{a2} = 4.77$, $pK_{a3} = 6.39$. Data taken from ref 39. ^bNot applicable.

presented in Figure 1. These molecules have varying octanol/water partition coefficient ($\log P$) and different protonation states as outlined in Table 1.

The structure of all small molecules was built using Chimera 1.5.3.⁴⁰ The parameters for each molecule used the CHARMM General Force Field (CGenFF)^{41–44} for organic molecules (program version 0.9.6 beta), translated into the GROMACS⁴⁵ format. The α -helical segment 1A (35 residues) of keratin 83 with a high contribution of charged residues (20% of basic, 11.43% of acidic) was built using the PyMol software.⁴⁶ The amino acid sequence was provided with the Human Intermediate Filament Database.⁴⁷ The keratin segment was minimized under vacuum, using the steepest descent (SD) algorithm.

To maintain consistency with our previous studies on keratin–EGCG, the CHARMM22/CMAP⁴⁸ force field with TIP3P⁴⁹ water model was used in all MD and SMD simulations

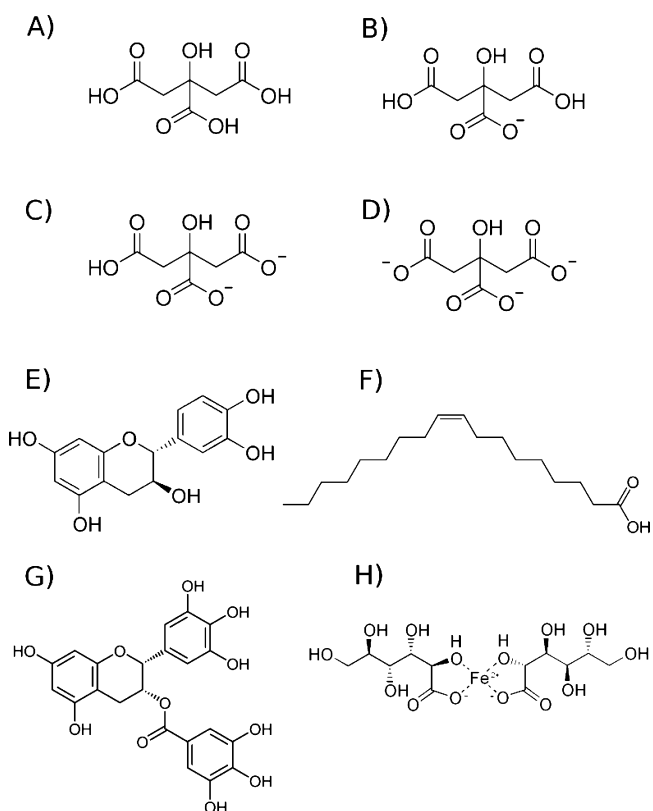


Figure 1. Molecules tested in this work: (A) citric acid, (B) dihydrogen citrate, (C) hydrogen citrate, (D) citrate, (E) catechin, and (F) oleic acid, as well as previously studied (G) epigallocatechin-3-gallate^{16,18} and (H) iron(II) gluconate.¹⁹

presented herein. All simulations were performed with the GROMACS 4.6⁴⁵ package compatible with graphics processing units (GPUs). With a time step of 2 fs, equations of motion were integrated through Verlet leapfrog algorithm. Bond lengths were constrained with the LINCS⁵⁰ algorithm. The cutoff distance was 1.4 nm for the short-range neighbor list and van der Waals interactions. The Particle Mesh Ewald method^{51,52} was applied for the long-range electrostatic interactions with a 1.4-m real space cutoff. The velocity rescale thermostat with additional stochastic term⁵³ and Parrinello–Rahman barostat⁵⁴ were used to maintain the temperature at 298 K and pressure at 1 bar. Initial velocities were set according to the Maxwell distribution. Periodic boundaries were used in all directions. All simulations were performed on two Linux clusters at Imperial College London: Department of Chemical Engineering Computing Service (URL: imperial.ac.uk/chemicalengineering) and High Performance Computing Service (URL: imperial.ac.uk/ict/services/teachingandresearchservices/highperformancecomputing).

Table 2. Details of MD Simulations for Keratin Segment 1A and Small Molecules at a Mass Concentration of 5%^a

system	ligand	pH	ref	number of ligand molecules	simulation time [ns]	temperature [K]
1	citric acid	<3.29	39	80	200	298
2	oleic acid	<8.5	55	55	200	298
3	catechin	<8.7	56	53	200	298
4	dihydrogen citrate/hydrogen citrate	4.5		52/28	200	298
5	citrate	>6.39	39	82	200	298

^aThe pH was set according to ligand pK_a values, which are provided in the reference.

GPUs (Geforce GTX680) were used for self-assembly simulations, and CPUs (Xeon E5–2620) were used for US and SMD simulations, respectively.

SYSTEM SETUP

α-Helix–Ligand Complexes. Initially, keratin segment 1A was placed at the center of a cubic unit cell size of 512 nm³ (8 nm × 8 nm × 8 nm). Terminal residues remained in their uncharged state. Small molecules were placed randomly around the keratin fragment to reach a mass concentration of 5%. The pH range (Table 2) corresponds to the ligand pK_a values and thus the most likely protonation state of the ligand. In system number 4 (Table 2), the pH was effectively fixed at ~4.5, corresponding to 65% of dihydrogen citrate, 35% of hydrogen citrate; this was represented by 52 and 28 molecules, respectively, at an overall mass concentration of 5%. The protein acidic and basic residues remained in their charged state in all simulations. The simulation box was filled with ~16 000 TIP3P water molecules and Na⁺ and Cl⁻ ions to neutralize the charge of the system. Energy minimization was then performed via the steepest descent algorithm. A two-step equilibration (0.2 ns each) in the canonical ensemble (NVT – constant number of atoms *N*, constant volume *V*, constant temperature *T*) and isothermal–isobaric ensemble (NPT – constant number of atoms *N*, constant pressure *P*, constant temperature *T*) was conducted, respectively. During the equilibration, positions of protein and ligand heavy atoms were restrained, allowing only water and ions to move in order to soak the system. The NPT ensemble at 298 K was used for the production simulation run of 200 ns. In total, five keratin–small molecule systems were investigated, as listed in Table 2.

In order to assess the type of interactions governing protein–ligand binding, the number of hydrogen bonds, as well as the overall hydrophobic surface area of small molecules, were calculated over the simulation time. Hydrogen bonds were based on the cutoff distance between the donor and the acceptor atoms below 0.35 nm and a hydrogen-donor–acceptor maximum angle of 30°. The overall hydrophobic area of small molecules was computed via numerical integration of their solvent-accessible surface area (SASA).⁵⁷ The buried area between protein and ligand was obtained by calculating the individual SASA of ligand, protein, and protein–ligand complex. The most-stable protein–ligand complex for each system was chosen based on the highest number of hydrogen bonds and the buried area. The protocol for those calculations is presented in the Results section.

Steered MD and Umbrella Sampling. For each simulation, the most-stable keratin–ligand complex was chosen for further SMD and free energy simulations. All other clustered layers of ligands as well as water and ions were removed from the system leaving only protein covered with the first layer of small molecules. This ensured consistency with our

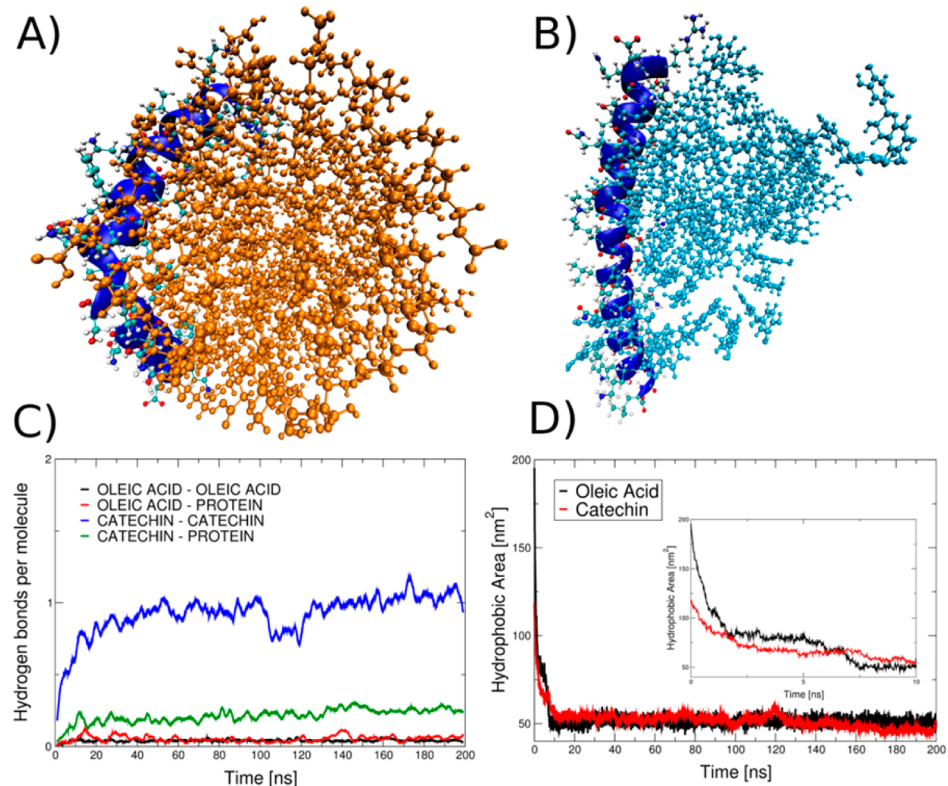


Figure 2. Final conformations of (A) oleic acids (orange) with keratin (blue) at 200 ns, and (B) catechin (cyan) with keratin (blue) at 200 ns. The mass concentration of ligand in both cases is 5%. (C) Number of hydrogen bonds between oleic acid–oleic acid, oleic acid–keratin, catechin–catechin, catechin–keratin over the simulation time. (D) Hydrophobic solvent-accessible surface area (SASA) of all catechin or oleic acid molecules, relative to the simulation time.

MD keratin–EGCG study¹⁶ (an excellent experimental agreement in binding affinity was reached) where no other molecules were present along the pulling pathway of EGCG. Subsequently, the protein with the first layer of small molecules was placed in a cubic box filled with TIP3P water and neutralizing ions. After energy minimization using SD, each keratin–small molecule system was equilibrated for 1 ns in the NVT and then the NPT ensemble. Based on the NPT equilibration phase, the ligand with the most stable interaction with protein (the greatest buried SASA and/or average number of hydrogen bonds) was chosen for further SMD and US studies. Subsequently, a constant velocity was applied to its COM and pulled 2–2.5 nm away, effectively into bulk solvent. In order to be consistent with the keratin–EGCG¹⁶ system, the pulling distance, direction (perpendicular to helical rod), and velocity of 10 nm ns⁻¹ were conserved. The influence of varying spring constants (from 1 kcal mol⁻¹ nm⁻² to 2000 kcal mol⁻¹ nm⁻²) on the rupture force was assessed by running 10 SMD replica simulations with a given spring constant of each protein–ligand complex. The measured rupture force corresponded to the arithmetic average over 10 independently obtained values.

SMD simulations were used to extract the initial coordinates for binding free energy calculations (US). In order to generate sufficient sampling, 0.1 nm spacing along the reaction coordinate (distance) was used. Each US window ran for 50 ns with a spring constant of 480 kcal mol⁻¹ nm⁻². The choice of the spring constant in each umbrella sampling window follows our previous study where the same spacing (0.1 nm) was used in the keratin helical segment interacting with ferrous ion,¹⁹ where excellent overlap of the histograms was attained.

The weighted histogram analysis method (WHAM)⁵⁸ was used to combine all windows into the PMF curve to estimate the binding free energy difference. Estimation of statistical error was performed for each PMF curve by dividing the entire trajectory of 50 ns into blocks of 10 ns.

RESULTS AND DISCUSSION

Keratin–Ligand Interactions. The number of hydrogen bonds between ligands and the keratin segment was calculated for each system over the 200 ns of simulation. In addition, for molecules with $\log P > 0$ (oleic acid and catechin, systems 2 and 3 in Table 2), only the number of hydrogen bonds between ligands was collected. The number of hydrogen bonds was divided by the total number of molecules and averaged over 1-ns windows for clarity (200 points). In order to observe possible hydrophobicity-driven interactions, the hydrophobic SASA of all catechin or oleic acid molecules was also calculated.

All oleic acid and catechin molecules rapidly clustered onto the keratin surface, forming a multilayer assembly (see Figures 2A and 2B), as previously observed for keratin–EGCG.^{16,18} In Figure 2D, the overall hydrophobic SASA of oleic acid and catechin is shown to decrease rapidly in the first 10 ns, because of cluster formation and binding to keratin. During this time, the hydrophobic SASA of oleic acid decreased from 200 nm² to 50 nm², whereas that of catechin decreased from 120 nm² to 48 nm². During the self-clustering and keratin binding process, the number of catechin–catechin hydrogen bonds per molecule increased to ~1 within 10 ns, supporting the multilayer assembly (Figure 2C). However, the number of hydrogen bonds per molecule within the catechin cluster and keratin

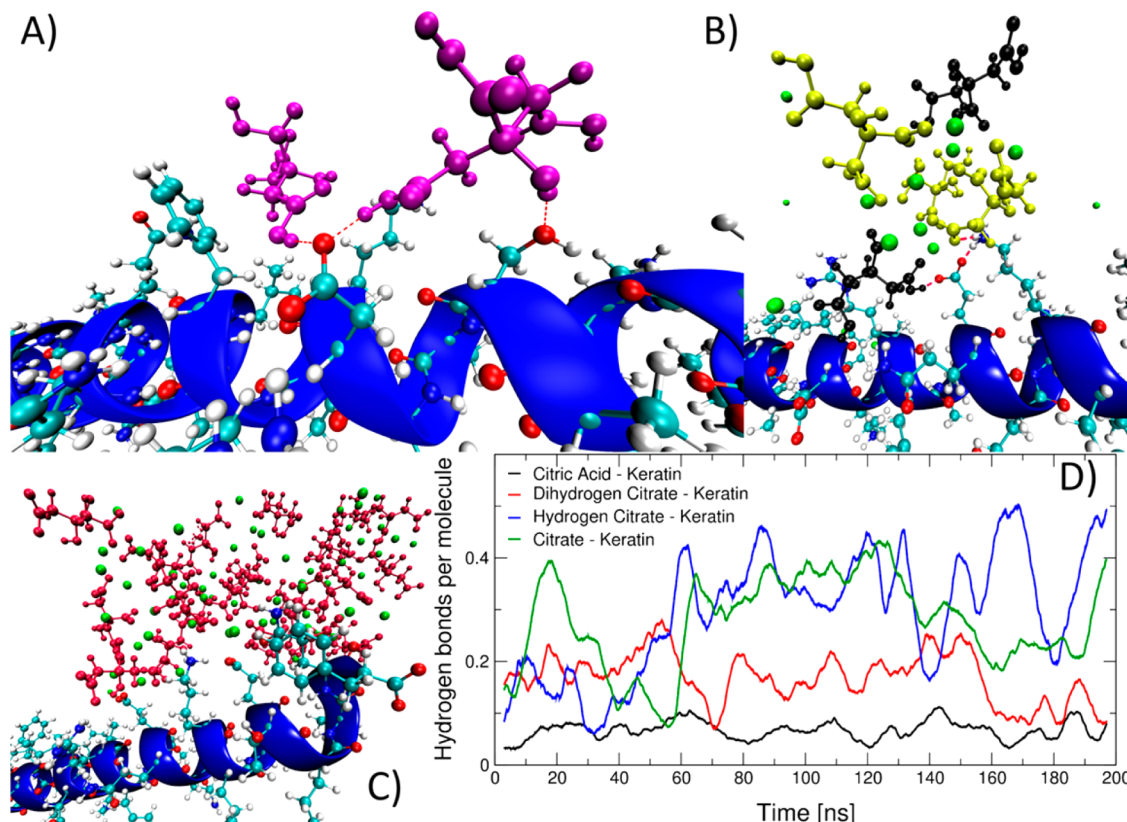


Figure 3. Citric acid binding to keratin at different pH values: (A) at pH < 3.29, citric acid binds to keratin via hydrogen bonds only; (B) at pH 4.5, hydrogen citrate and dihydrogen citrate formed small salt aggregates via Na^+ ions and stacked on the keratin surface via hydrogen bonds and electrostatic interactions; (C) at pH > 6.39, citrate formed a salt cluster of 26 molecules stabilized by Na^+ ions, mediating the interactions between citrate molecules as well as citrate–keratin charged residues. (D) Number of hydrogen bonds over the simulation time (averaged over 200 data points every 1 ns). [Legend of atoms for helical keratin: red, oxygen; blue, nitrogen; cyan, carbon; white, hydrogen; purple, citric acid; black, dihydrogen citrate; yellow, hydrogen citrate; green, Na^+ ions; and blue, cartoon representation of protein.]

varied at ~ 0.25 (Figure 2C). This shows that, in addition to hydrophobic interactions, hydrogen bonding is also involved in the process of binding to keratin, which is consistent with the presence of 6 potential hydrogen bond acceptors, and 5 hydrogen bond donors in catechin, as well as its log P value of 0.51.³⁷ For oleic acid clusters, the number of hydrogen bonds per molecule remained below 0.1 throughout the simulation. Similarly, the number of hydrogen bonds between the oleic acid assemblies and keratin was low, suggesting that hydrophobic interactions dominate. The log P value of 7.64 for oleic acid, as well as the presence of only two hydrogen bond acceptors and one donor, supports our observations of hydrophobic assembly as the main driving force.

For citric acid, hydrogen citrate/dihydrogen citrate, and citrate (systems 1, 4, and 5 in Table 2), the number of hydrogen bonds between ligands and keratin was calculated over the simulation time (see Figure 3D). Citric acid had the smallest number of hydrogen bonds per molecule (Figure 3A). The increase of the overall charge (dihydrogen citrate of -1 , hydrogen citrate of -2 , citrate of -3) resulted in an increase in the number of hydrogen bonds. At pH 4.5 (system 4 in Table 2), hydrogen citrate and dihydrogen citrate formed small salt clusters (2–5) via ionic bonds mediated by Na^+ ions (see Figure 3B). This led to stronger interactions, in comparison to citric acid. For citrate (system 5 in Table 2), electrostatic interactions were dominant. It was observed (Figure 3C) that 26 citrate molecules formed a salt aggregate stabilized by Na^+ ions.

During each protein–ligand binding process, the α -helical keratin segment did not undergo any conformational changes. In Figure S1 in the Supporting Information, an example of the maintenance of the polypeptide backbone secondary structure during the catechin binding process is presented.

Identifying the Most-Stable Ligand-Bound State. From each MD simulation, all the molecules directly bound to the keratin surface were assessed in terms of stability. All the clustered layers of small molecules that did not directly interact with the keratin surface were omitted. The assessment of stability was based on the average number of hydrogen bonds and the buried surface area between ligand and protein. The protocol for the choice of the most stable configurations is presented in Figure 4, using catechin as an example.

From the last frame at 200 ns, all the catechins being directly attached to keratin were selected (see Figure 4A; red and green surfaces represent catechins). Subsequently, the average number of hydrogen bonds between each molecule and keratin were calculated over the last 50 ns of the simulation time and averaged (Figure 4B). Two molecules (green surface representation in Figure 4A) were observed to have the highest average number of hydrogen bonds and were further analyzed in terms of keratin–ligand buried area (Figure 4C). It appeared that the molecule labeled Catechin_38 exhibited the greatest buried area with keratin and, hence, was chosen as the most stable configuration and used for SMD and free energy simulations (US). The choice of this keratin–catechin complex is further confirmed by the three hydrogen bonds formed with

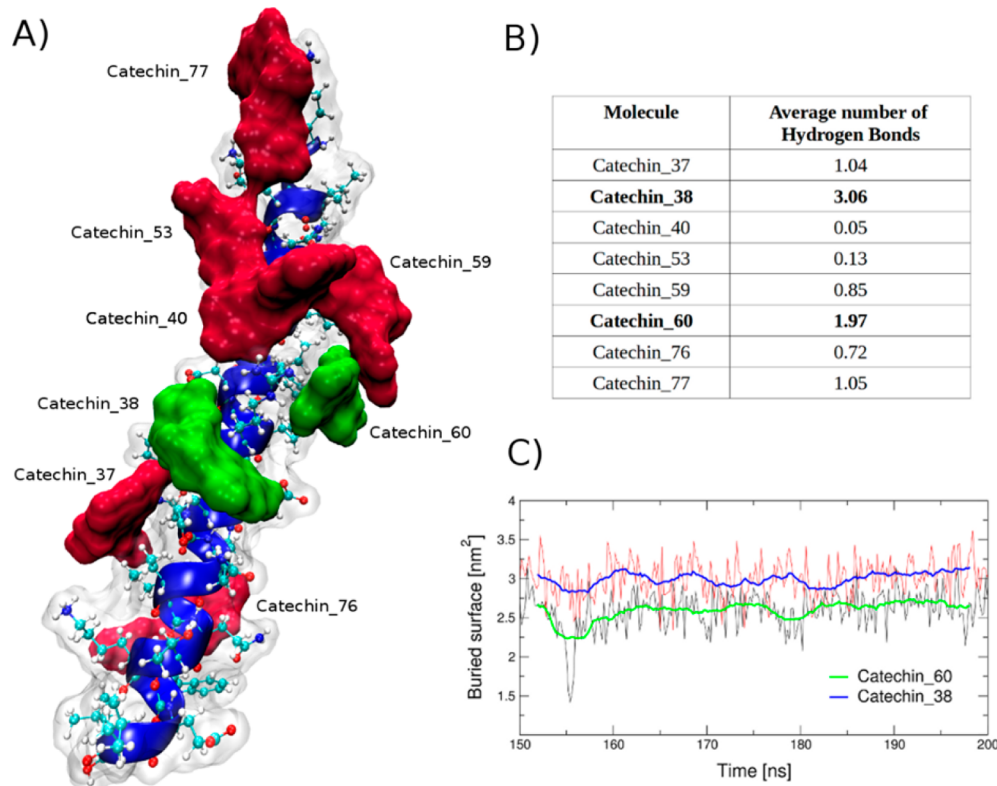


Figure 4. Protocol employed for choosing the most-stable α -helix ligand-bound coordinates using catechin as an example: (A) 200-ns snapshot of the molecules that are directly bound to the keratin (green surface represents catechins with the highest number of hydrogen bonds and red surface represents the remaining catechins). [Legend of atoms for helical keratin: red, oxygen; blue, nitrogen; cyan, carbon; white, hydrogen.] (B) The average number of hydrogen bonds calculated over last 50 ns for all molecules interacting with keratin surface; (C) The keratin–catechin buried surface area calculated for two molecules that exhibited the highest number of hydrogen bonds.

Table 3. Keratin α -Helix–Ligand Complex Binding Data^a

molecule name	ΔG_{MD} [kcal/mol]	ΔG_{Exp} [kcal/mol]	protein–ligand buried surface [nm ²]	rupture force [kcal mol ⁻¹ nm ⁻¹]
oleic acid	-9.56 ± 0.4	-9.45 (ref 64) / -10.16 (ref 65)	5.91	46.54 ± 10
EGCG	-6.20 ± 0.2	-6.37 (ref 18)		
catechin	-3.30 ± 0.3	-2.87 (ref 66)	2.94	61.78 ± 10
citric acid	-0.66 ± 0.2		1.99	39.44 ± 8
dihydrogen citrate	-1.26 ± 0.2			44.54 ± 8
hydrogen citrate	-2.70 ± 0.2			72.12 ± 9
citrate	-4.50 ± 0.3	-5.30 (ref 67)		189.59 ± 20
Fe^{2+}	-7.20 ± 0.2	-7.43 (ref 19)		248.67 ± 25

^aBinding free energies from umbrella sampling (ΔG_{MD}); binding free energies validated experimentally (for EGCG and Fe^{2+}) and experimentally obtained with other proteins (ΔG_{Exp}); buried surface area of uncharged molecules; rupture force obtained as the average value over 10 identical pulling simulations at the constant loading rate (velocity of 10 nm ns^{-1} and spring constant of $120\text{ kcal mol}^{-1}\text{ nm}^{-2}$) according to the keratin–EGCG study.

keratin (a total of five possible hydrogen bond donors exist per catechin) as well as the total of 3 nm^2 of area buried between protein and ligand (in comparison with a total of 4 nm^2 surface area for an isolated catechin molecule). This stability-protocol assessment was employed for oleic acid, citric acid, hydrogen citrate, dihydrogen citrate, and citrate. The keratin– Fe^{2+} coordinates for SMD protocol were taken from our previous study.¹⁹

Steered Molecular Dynamics (SMD) and Umbrella Sampling (US). Each system consisted of keratin and the first layer of small molecules directly bound to keratin. The remaining clustered ligand molecules were removed in order to be consistent with our previous study, where no other molecules were present along the pulling pathway. Prior to the

pulling simulations, from a 1-ns system equilibration simulation (in the NPT ensemble), mean values of protein–ligand buried surface area for uncharged molecules (catechin, citric acid, oleic acid) were obtained and are listed in Table 3. Pulling simulations were performed at a range of spring constants. An example of pulling simulation of the most stably bound catechin is shown in Figure 5. The pulling direction, as in our previous study,¹⁶ was perpendicular to the helical backbone axis. During the SMD simulation, the force reached the maximum (rupture force) at $\sim 0.1\text{ nm}$, where the last hydrogen bond was broken. The distance between the catechin and keratin segment COM started increasing at the same time, reaching 2.4 nm by the end of the simulation. In all SMD simulations, the helical secondary structure of the polypeptide

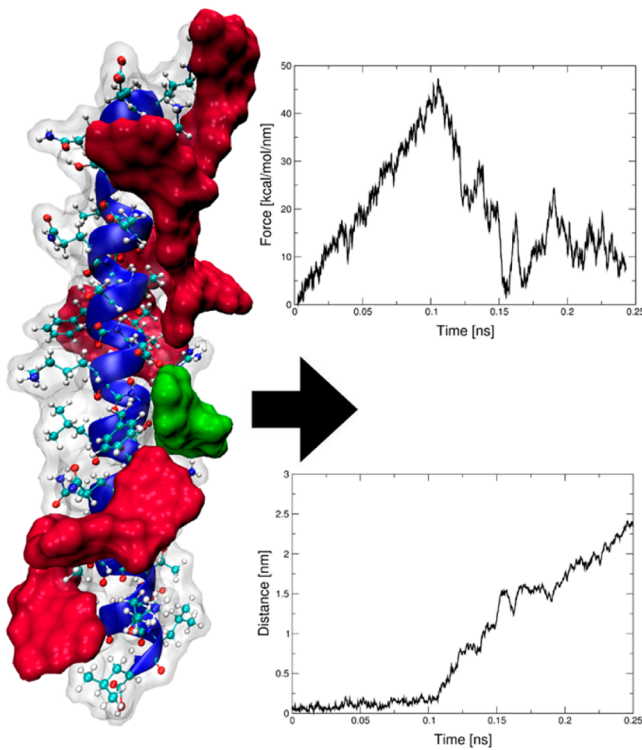


Figure 5. Example of pulling simulation of catechin (green surface representation) from keratin. The pulling direction according to our previous study¹⁶ is perpendicular to the helical backbone axis. During the SMD simulation at ~ 0.1 ns, the force reaches the maximum when the last hydrogen bond is broken. The distance between the keratin helical segment and the catechin starts increasing at this point, reaching 2.4 nm by the end of the simulation. Red surface represents the remaining catechins obtained by MD self-assembly simulations; white surface represents helical keratin. [Legend of atoms for helical keratin: red, oxygen; blue, nitrogen; cyan, carbon; white, hydrogen.]

segment remained remarkably stable throughout the simulation; an example for the citric acid secondary structure stability during SMD is presented in Figure S2 in the Supporting Information.

Results from the SMD protocol are presented in Figure 6. Those results correspond to simulations starting from the most stably bound ligand coordinates assessed in the previous step. The plots represent the maximum pulling force (rupture force) averaged over 10 replica pulling simulations versus the chosen harmonic spring constant. The error was estimated as the maximum and minimum of the obtained 10 rupture forces for a given spring constant. It was observed that the increase in the stiffness of the spring resulted in an increase in the maximum pulling force, as expected. This relationship is theoretically described by an exponential function^{31–34} derived from the Bell model,³⁰ and our results correlated with such dependency ($R^2 = 0.90\text{--}0.94$). However, even better results were obtained with the power function ($R^2 = 0.96\text{--}0.98$). This likely arises from the fast pulling velocity of 10 nm ns^{-1} used in simulations in comparison to AFM or dynamic force spectroscopy experimental studies, where the limit of exponential dependency is reached.^{59–63}

SMD trajectories provided the initial configurations for US windows which were equally spaced in 0.1 nm windows, yielding a total of 21–27 windows of 50 ns each. The free energy of binding (PMF) is the difference between the minima where the small molecule is adsorbed to the protein and the

plateau value when interactions are effectively absent (Figure 7). The umbrella sampling histograms of each molecule are shown in the Supporting Information (Figure S3), presenting excellent overlap. The free energies of molecular binding to the keratin α -helical segment obtained via US are listed in Table 3 (ΔG_{MD}) and are compared with available experimentally determined (ITC) results (ΔG_{Exp}) binding other proteins or directly validated (EGCG, ferrous ion). The binding free energies from US exhibit a good agreement with experimental results. The highest magnitude ($\Delta G = -9.56 \text{ kcal mol}^{-1}$) of binding free energy was obtained for oleic acid, which has the highest octanol/water partition coefficient ($\log P = 7.64$).

Figure 8A shows the binding free energy difference from US versus the $\log P$ values of uncharged molecules studied herein. It was observed that the higher the $\log P$ value, the greater the magnitude of the binding free energy, which is consistent with hydrophobic interactions being the main driving force for assembly. It may also be noted that an effective increase in pH resulted in an increase of binding free energy for citric acid. The increase of the pH above the respective pK_a values results in a decrease of the overall charge and, hence, stronger electrostatic interaction with keratin (Figure 8B). Finally, the correlation of the buried area (circle data points from keratin–EGCG study¹⁶) for uncharged molecules (oleic acid, catechin and citric acid), as a function of the free energy, is presented in Figure 8C. A strong correlation was observed, and, in general, the higher the buried area between the α -helix and the ligand, the stronger the binding affinity.

Our main goal from this study was to assess the validity of the linear dependency observed originally for the keratin–EGCG system,¹⁶ extended to the rupture force versus binding free energy for each of the 7 ligands studied herein. For this purpose, the rupture force for each molecule was extracted as an average value over 10 SMD trajectories, with a spring constant of $120 \text{ kcal mol}^{-1} \text{ nm}^{-2}$ (according to the keratin–EGCG study¹⁶). Mean rupture force values for each molecule, together with standard deviations, are listed in Table 3. In Figure 9, these rupture forces are presented versus the binding free energies obtained from US. Not all molecules studied here followed the same linear correlation that we observed previously.¹⁶ Thus, two linear correlations could be identified. The first linear model (Figure 9, black line) obtained from the keratin–EGCG study¹⁶ has been extended for molecules whose binding interactions with keratin are governed by hydrogen bonding and/or a combination of hydrogen bonding and hydrophobic interaction: citric acid and catechin respectively ($R^2 = 0.98$). A second (Figure 9, red line) slightly weaker linear correlation ($R^2 = 0.94$) was observed for charged molecules whose interactions with the α -helix are driven by electrostatics (dihydrogen citrate, hydrogen citrate, citrate, and ferrous ion). The uncharged oleic acid (Figure 9, blue spherical point) did not follow either of the two correlations, because of its assembly process, which proceeded primarily via hydrophobic interaction with the α -helix, where hydrogen bonds or electrostatics were not present. It is likely that a third linear correlation may be derived for molecules interacting with keratin via hydrophobic collapse only.

Predicting the binding free energy by SMD simulations offers both advantages and disadvantages. The key point is that SMD simulations are much shorter (hundreds of picoseconds to nanoseconds each), saving significant computational time in comparison to free energy methods where extensive sampling (hundreds of nanoseconds each) is required. However, the

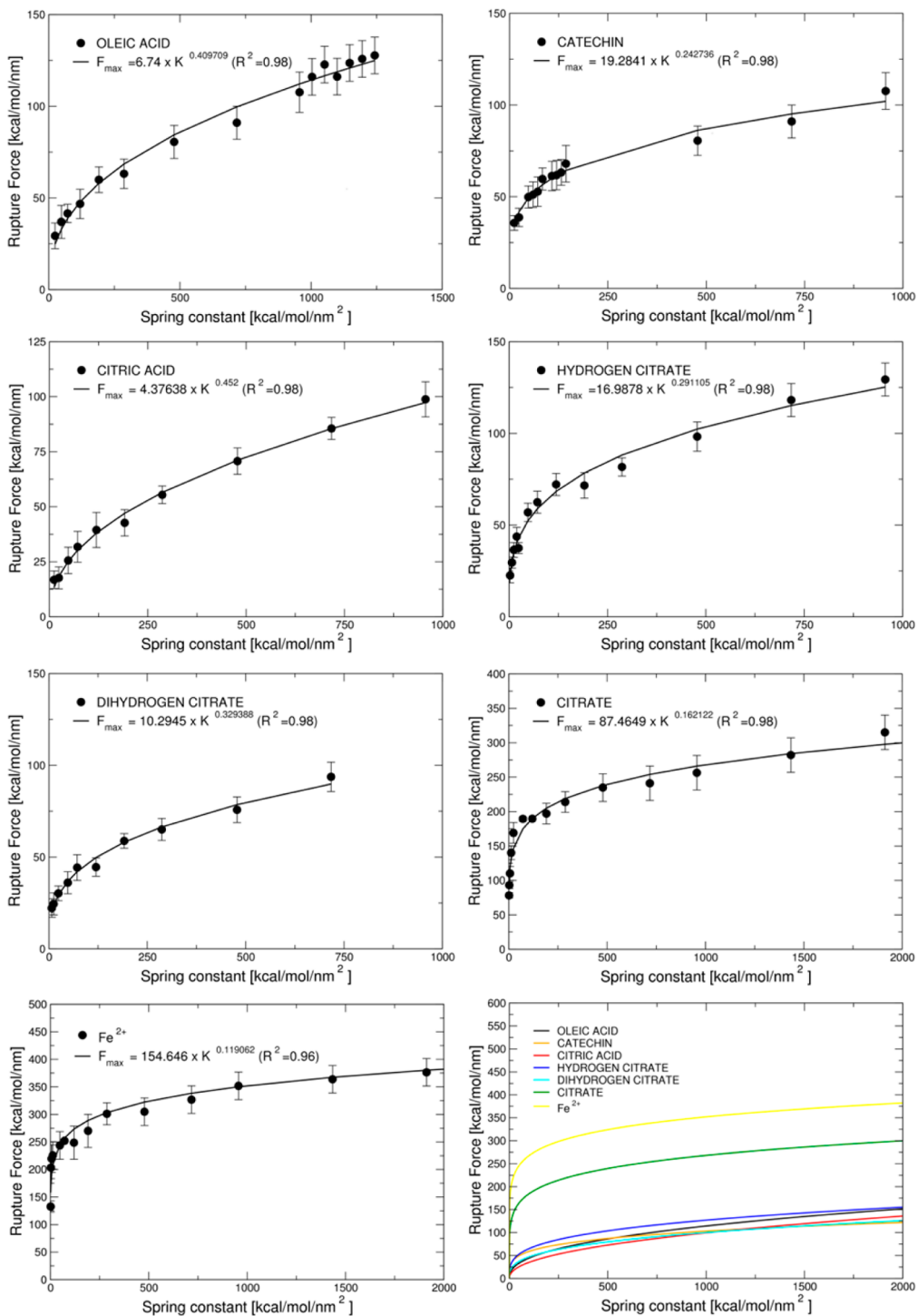


Figure 6. Rupture force obtained from steered molecular dynamics (SMD) simulations for 7 molecules (oleic acid, catechin, citric acid, dihydrogen citrate, hydrogen citrate, citrate, and ferrous ion) versus the used spring constant. Each point corresponds to the average value of 10 identical pulling simulations. The best-fitted curve was obtained in each case with a power function of $R^2 = 0.96–0.98$.

linear correlation models of free energy predictions have been applied herein to small molecules interacting with a stable α -helical surface. This has not been implemented and assessed for complex proteins where significant conformational changes upon ligand binding process are possible, or where the binding site is deeply buried. The fundamental errors associated with using SMD simulation to predict free energies lie mainly in the rupture force (see Figure 9 and Table 3). Linear correlations derived for molecules interacting via hydrogen bonds/hydro-

phobic interactions appears to be very accurate ($R^2 = 0.98$) and the errors associated with the rupture force remain within ± 10 kcal mol $^{-1}$ nm $^{-1}$, which provides an estimate of the free energy error of ~ 1 kcal mol $^{-1}$. For electrostatics-governed interactions, the error corresponds to ± 25 kcal mol $^{-1}$ nm $^{-1}$ for the ferrous ion and ± 20 kcal mol $^{-1}$ nm $^{-1}$ for citrate, which also remain within the ± 1 kcal mol $^{-1}$ estimation of the free energy. In the future, the validity of the observed linear models needs to be further tested for a larger number of ligands with a wide

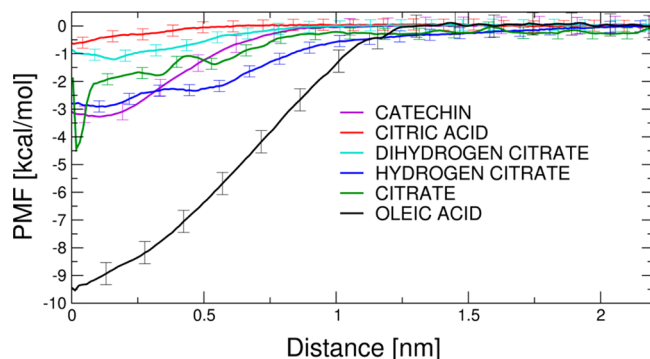


Figure 7. Potential of mean force obtained from umbrella sampling for different molecules binding to the keratin helical segment.

chemical space, and for other proteins not limited to surface-exposed α -helical motifs, while the effects of structural changes also remain to be investigated. Nevertheless, as a proof of principle, this study shows that establishing linear correlations between free energies and rupture forces could provide a promising methodology for fast free energy predictions for binding of related small molecular series.

CONCLUSIONS

The binding affinity of small molecules to biological macromolecules is an important thermodynamic property. Recent advances in molecular dynamics (MD) simulations enable prediction of binding free energy with high accuracy. However, quantitative methods within an MD simulation framework involving explicit solvent are computationally very demanding. In previous work on the α -helix–epigallocatechin-3-gallate (α -helix–EGCG) system, a linear dependency between the binding free energy (obtained from extensive umbrella sampling (US)) and the rupture force (obtained from short steered molecular dynamics (SMD) simulations) was presented. Previous work of Mai et al.^{26,27} on swine influenza A/H1N1 virus also suggested a linear correlation between the binding free energy and the maximum pulling force for different ligands. For the first time, in this study, the generality of the linear binding model is tested for several ligands with varying physicochemical properties.

Initially, the type of interactions involved in the binding process was assessed. This involved hydrophobic interactions for neutral oleic acid, electrostatic interactions for citrate, hydrophobic interactions and hydrogen bonding for catechin, as well as a combination of hydrogen bonds and electrostatics for hydrogen citrate and dihydrogen citrate. Subsequently, for each molecule (the most stable keratin–ligand conformation) using the SMD protocol, a correlation of rupture force versus applied spring constant was established. Although this dependency in the context of atomic force microscopy (AFM) experimental data is often described by the logarithmic function according to the Bell model, our higher-velocity SMD simulations agreed best with the power function. Subsequently, the binding affinity of each molecule for the keratin helix was calculated using US, yielding close agreement with available experimental data. Finally, the validity of the keratin–EGCG linear correlation of rupture force versus the free energy was assessed. Not all molecules studied herein followed the same linear model as for EGCG–keratin system. The linear correlation for keratin–EGCG could only be extended for molecules where interactions are dominated by hydrogen

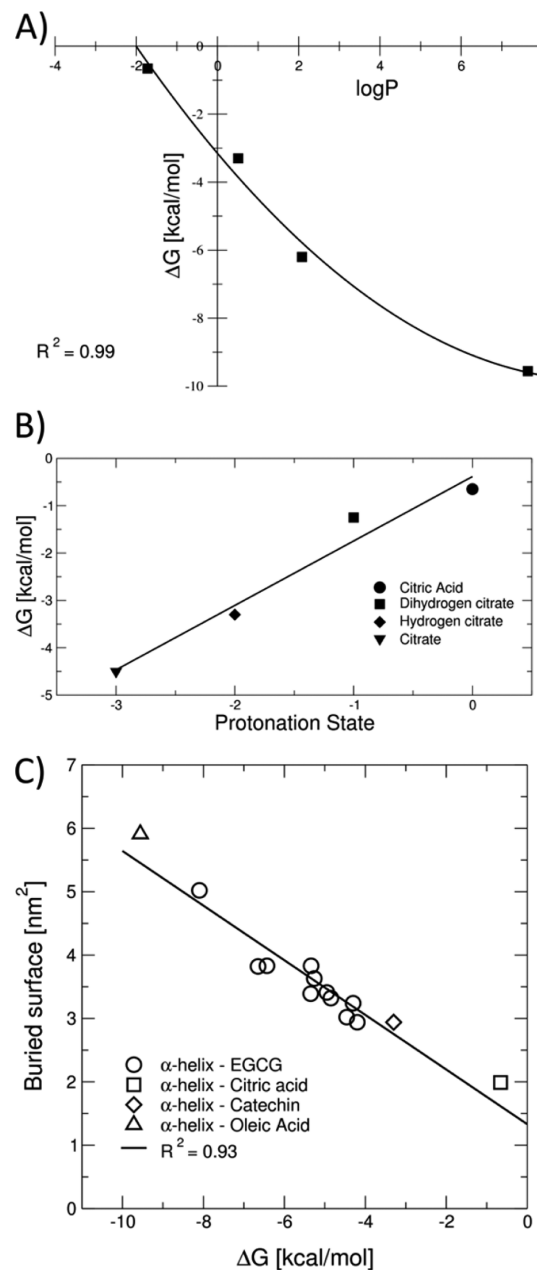


Figure 8. (A) Binding free energy (ΔG) of small neutral molecules to the helical motif as a function of $\log P$. (B) Binding free energy of citric acid at different protonation states. (C) Protein–ligand buried area (A), as a function of the binding free energy for neutral molecules. The equation is best described by $A = 1.3321 - 0.431\Delta G$.

bonds (citric acid) or a combination of hydrogen bonds and hydrophobic forces (catechin). However, a second linear correlation could be demonstrated for charged molecules interacting primarily via electrostatics (dihydrogen citrate, hydrogen citrate, citrate, and ferrous ion). Uncharged oleic acid did not follow any linearity, because of the fact that its interaction with keratin was dominated by hydrophobic forces. Although not assessed in this study, it is very possible that a third linear correlation exists for molecules interacting with keratin via hydrophobic assembly. Irrespective of the limited chemical space investigated here, our short SMD simulation-based methodology represents a promising tool for fast free energy predictions (requiring picoseconds to nanoseconds of

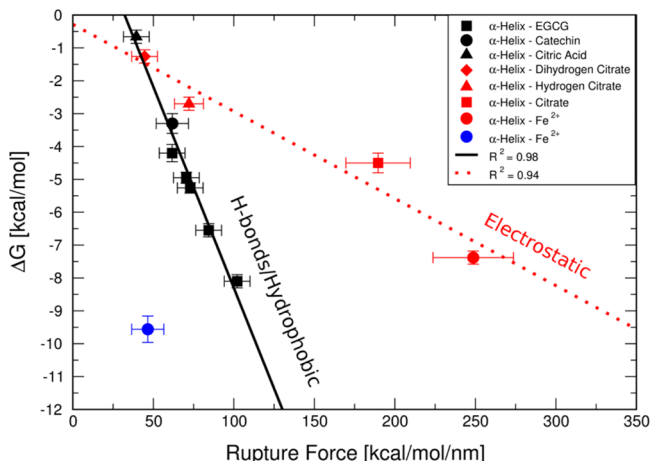


Figure 9. Binding free energies (ΔG) obtained from US of small molecules interacting with the keratin helical motif versus the rupture force averaged over 10 SMD simulations at constant loading rate according to the keratin-EGCG study.¹⁶ Two linear dependencies were obtained: (1, black line and data points) for molecules interacting via either hydrogen bonding or combination of hydrogen bonding and hydrophobic collapse (EGCG, catechin, citric acid) with $R^2 = 0.98$ ($\Delta G = -0.122F_{\text{Max}} + 3.94$); (2, red line and data point) for charged molecules interacting via electrostatic interactions (dihydrogen citrate, hydrogen citrate, citrate, and ferrous ion) with $R^2 = 0.94$ ($\Delta G = -0.027F_{\text{Max}} + 0.28$). Neutral oleic acid (blue), in which interactions with the α -helix are governed by hydrophobic forces and did not follow either linear series.

sampling) in comparison with rigorous free energy methods (typically requiring nanosecond to microsecond time scale sampling) that may be extended to more-complex systems in the future.

ASSOCIATED CONTENT

Supporting Information

The example of the maintenance of the keratin secondary structure during the self-assembly and pulling simulation is presented in Figure S1 and S2 respectively. Umbrella sampling histograms are presented in Figure S3. This material is available free of charge via the Internet at <http://pubs.acs.org>.

AUTHOR INFORMATION

Corresponding Authors

*E-mail: guoping.lian@unilever.com (G. Lian).

*E-mail: a.mantalaris@imperial.ac.uk (A. Mantalaris).

Notes

The authors declare no competing financial interest.

ACKNOWLEDGMENTS

The research leading to these results has received funding from the EC's Seventh Framework Programme [FP7/2007-2013] under Grant Agreement No. 238013, which is greatly acknowledged. The first author wishes to acknowledge Prof. Daan Frenkel, Prof. Pablo Debenedetti, Dr. Robert Farr, Dr. Janhavi Raut, Dr. Alfonso De Simone, and Dr. Daniel Holdbrook for stimulating discussions, as well as Crombie Terrance and Matt Harvey, together with High Performance Computing Service at Imperial College London for the technical support.

REFERENCES

- Beveridge, D. L.; Dicapua, F. M. Free Energy Via Molecular Simulation—Applications to Chemical and Biomolecular Systems. *Annu. Rev. Biophys. Chem.* **1989**, *18*, 431–492.
- Deng, Y. Q.; Roux, B. Computations of Standard Binding Free Energies with Molecular Dynamics Simulations. *J. Phys. Chem. B* **2009**, *113*, 2234–2246.
- Talhout, R.; Villa, A.; Mark, A. E.; Engberts, J. B. Understanding binding affinity: a combined isothermal titration calorimetry/molecular dynamics study of the binding of a series of hydrophobically modified benzamidinium chloride inhibitors to trypsin. *J. Am. Chem. Soc.* **2003**, *125*, 10570–10579.
- Dubey, K. D.; Tiwari, R. K.; Ojha, R. P. Recent Advances in Protein–Ligand Interactions: MD Simulations and Binding Free Energy. *Curr. Comput. Aided Drug Des.* **2013**, *9*, 518–531.
- Anisimov, V. M.; Ziemys, A.; Kizhake, S.; Yuan, Z.; Natarajan, A.; Cavasotto, C. N. Computational and experimental studies of the interaction between phospho-peptides and the C-terminal domain of BRCA1. *J. Comput. Aided Mol. Des.* **2011**, *25*, 1071–1084.
- Kollman, P. A.; Massova, I.; Reyes, C.; Kuhn, B.; Huo, S. H.; Chong, L.; Lee, M.; Lee, T.; Duan, Y.; Wang, W.; Donini, O.; Cieplak, P.; Srinivasan, J.; Case, D. A.; Cheatham, T. E. Calculating structures and free energies of complex molecules: Combining molecular mechanics and continuum models. *Acc. Chem. Res.* **2000**, *33*, 889–897.
- Kuhn, B.; Gerber, P.; Schulz-Gasch, T.; Stahl, M. Validation and use of the MM-PBSA approach for drug discovery. *J. Med. Chem.* **2005**, *48*, 4040–4048.
- Hansson, T.; Marelius, J.; Aqvist, J. Ligand binding affinity prediction by linear interaction energy methods. *J. Comput. Aided Mol. Des.* **1998**, *12*, 27–35.
- Laio, A.; Parrinello, M. Escaping free-energy minima. *Proc. Natl. Acad. Sci. U. S. A.* **2014**, *99*, 12562–12566.
- Kokubo, H.; Tanaka, T.; Okamoto, Y. Ab initio prediction of protein-ligand binding structures by replica-exchange umbrella sampling simulations. *J. Comput. Chem.* **2011**, *32*, 2810–2821.
- Torrie, G. M.; Valleau, J. P. Monte-Carlo Free-Energy Estimates Using Non-Boltzmann Sampling—Application to Subcritical Lennard-Jones Fluid. *Chem. Phys. Lett.* **1974**, *28*, 578–581.
- Torrie, G. M.; Valleau, J. P. Non-Physical Sampling Distributions in Monte-Carlo Free-Energy Estimation—Umbrella Sampling. *J. Comput. Phys.* **1977**, *23*, 187–199.
- Buch, I.; Sadiq, S. K.; De Fabritiis, G. Optimized Potential of Mean Force Calculations for Standard Binding Free Energies. *J. Chem. Theory Comput.* **2011**, *7*, 1765–1772.
- Chen, P. C.; Kuyucak, S. Accurate Determination of the Binding Free Energy for KcsA-Charybdotoxin Complex from the Potential of Mean Force Calculations with Restraints. *Biophys. J.* **2011**, *100*, 2466–2474.
- Feeenstra, P.; Brunsteiner, M.; Khinast, J. Prediction of drug-packaging interactions via molecular dynamics (MD) simulations. *Int. J. Pharm.* **2012**, *431*, 26–32.
- Marzinek, J. K.; Zhao, Y.; Lian, G.; Mantalaris, A.; Pistikopoulos, E. N.; Bond, P. J.; Noro, M. G.; Han, L.; Chen, L. Molecular and thermodynamic basis for EGCG–Keratin interaction—Part I: Molecular dynamics simulations. *AIChE J.* **2013**, *59*, 4816–4823.
- Woo, H. J.; Roux, B. Calculation of absolute protein–ligand binding free energy from computer simulations. *Proc. Natl. Acad. Sci. U. S. A.* **2005**, *102*, 6825–6830.
- Zhao, Y.; Marzinek, J. K.; Chen, L.; Mantalaris, A.; Pistikopoulos, E. N.; Han, L.; Lian, G.; Bond, P. J.; Noro, M. G. Molecular and Thermodynamic Basis for EGCG–Keratin Interaction—Part II: Experimental Investigation. *AIChE J.* **2013**, *59*, 4824–4827.
- Zhao, Y.; Marzinek, J. K.; Bond, P. J.; Chen, L.; Li, Q.; Mantalaris, A.; Pistikopoulos, E. N.; Noro, M. G.; Han, L.; Lian, G. A study on Fe^{2+} –alpha helical rich keratin complex formation using isothermal titration calorimetry and molecular dynamics simulation. *J. Pharm. Sci.* **2014**, *103*, 1224–1232.

- (20) Izrailev, S.; Stepaniants, S.; Schulten, K. Applications of steered molecular dynamics to protein-ligand/membrane binding. *Biophys. J.* **1998**, *74*, A177.
- (21) Yu, T.; Lee, O. S.; Schatz, G. C. Steered molecular dynamics studies of the potential of mean force for Peptide amphiphile self-assembly into cylindrical nanofibers. *J. Phys. Chem. A* **2013**, *117*, 7453–7460.
- (22) He, J.; Xu, L.; Zhang, S.; Guan, J.; Shen, M.; Li, H.; Song, Y. Steered molecular dynamics simulation of the binding of the beta2 and beta3 regions in domain-swapped human cystatin C dimer. *J. Mol. Model.* **2013**, *19*, 825–832.
- (23) Skovstrup, S.; David, L.; Tabouret, O.; Jorgensen, F. S. A steered molecular dynamics study of binding and translocation processes in the GABA transporter. *PLoS One* **2012**, *7*, e39360.
- (24) Li, M. S.; Mai, B. K. Steered Molecular Dynamics—A Promising Tool for Drug Design. *Curr. Bioinform.* **2012**, *7*, 342–351.
- (25) Jarzynski, C. Nonequilibrium equality for free energy differences. *Phys. Rev. Lett.* **1997**, *78*, 2690–2693.
- (26) Mai, B. K.; Viet, M. H.; Li, M. S. Top Leads for Swine Influenza A/H1N1 Virus Revealed by Steered Molecular Dynamics Approach. *J. Chem. Inf. Model.* **2010**, *50*, 2236–2247.
- (27) Mai, B. K.; Li, M. S. Neuraminidase inhibitor R-125489—A promising drug for treating influenza virus: Steered molecular dynamics approach. *Biochem. Biophys. Res. Commun.* **2011**, *410*, 688–691.
- (28) Stickle, D. F.; Presta, L. G.; Dill, K. A.; Rose, G. D. Hydrogen-Bonding in Globular-Proteins. *J. Mol. Biol.* **1992**, *226*, 1143–1159.
- (29) Pace, C. N.; Scholtz, J. M. A helix propensity scale based on experimental studies of peptides and proteins. *Biophys. J.* **1998**, *75*, 422–427.
- (30) Bell, G. I. Theoretical-Models for the Specific Adhesion of Cells to Cells. *Science* **1978**, *200*, 618–627.
- (31) Izrailev, S.; Stepaniants, S.; Balsera, M.; Oono, Y.; Schulten, K. Molecular dynamics study of unbinding of the avidin–biotin complex. *Biophys. J.* **1997**, *72*, 1568–1581.
- (32) Sekatskii, S. K.; Benedetti, F.; Dietler, G. Dependence of the most probable and average bond rupture force on the force loading rate: First order correction to the Bell–Evans model. *J. Appl. Phys.* **2013**, *114*, 034701.
- (33) Husson, J.; Pincet, F. Analyzing single-bond experiments: Influence of the shape of the energy landscape and universal law between the width, depth, and force spectrum of the bond. *Phys. Rev. E* **2008**, *77*, 026108.
- (34) Dudko, O. K.; Hummer, G.; Szabo, A. Intrinsic rates and activation free energies from single-molecule pulling experiments. *Phys. Rev. Lett.* **2006**, *96*, 108101.
- (35) Sangster, J. Octanol–Water Partition-Coefficients of Simple Organic-Compounds. *J. Phys. Chem. Ref. Data* **1989**, *18*, 1111–1229.
- (36) ChemSpider, CSID: 58575. <http://www.chemspider.com/Chemical-Structure.58575.html> (accessed April 18, 2014).
- (37) Perrissoud, D.; Testa, B. Inhibiting or Potentiating Effects of Flavonoids on Carbon Tetrachloride-Induced Toxicity in Isolated Rat Hepatocytes. *Arzneim.-Forsch.* **1986**, *36*, 1249–1253.
- (38) ChemSpider—The free chemical database. Accessible via the Internet at <http://www.chemspider.com>; ID 305, 2013.
- (39) Data for Biochemical Research. ZirChrom Separations, Inc.; Retrieved Jan. 11, 2012.
- (40) Pettersen, E. F.; Goddard, T. D.; Huang, C. C.; Couch, G. S.; Greenblatt, D. M.; Meng, E. C.; Ferrin, T. E. UCSF chimera—A visualization system for exploratory research and analysis. *J. Comput. Chem.* **2004**, *25*, 1605–1612.
- (41) ParamChem Interface; available via the Internet at <https://www.paramchem.org>.
- (42) Vanommeslaeghe, K.; Hatcher, E.; Acharya, C.; Kundu, S.; Zhong, S.; Shim, J.; Darian, E.; Guvench, O.; Lopes, P.; Vorobyov, I.; MacKerell, A. D. CHARMM General Force Field: A Force Field for Drug-Like Molecules Compatible with the CHARMM All-Atom Additive Biological Force Fields. *J. Comput. Chem.* **2010**, *31*, 671–690.
- (43) Vanommeslaeghe, K.; Ghosh, J.; Polani, N. K.; Sheetz, M.; Pamidighantam, S. V.; Connolly, J. W. D.; MacKerell, A. D. Automation of the Charmm General Force Field for Drug-Like Molecules. *Biophys. J.* **2011**, *100*, 611a–611a.
- (44) Vanommeslaeghe, K.; Raman, E. P.; MacKerell, A. D. Automation of the CHARMM General Force Field (CGenFF) II: Assignment of Bonded Parameters and Partial Atomic Charges. *J. Chem. Inf. Model.* **2012**, *52*, 3155–3168.
- (45) Hess, B.; Kutzner, C.; van der Spoel, D.; Lindahl, E. GROMACS 4: Algorithms for Highly Efficient, Load-Balanced, and Scalable Molecular Simulation. *J. Chem. Theory Comput.* **2008**, *4*, 435–447.
- (46) The PyMOL. Molecular Graphics System, Version 1.5.0.4; Schrödinger, LLC, 2012.
- (47) Szeverenyi, I.; Cassidy, A. J.; Chung, C. W.; Lee, B. T.; Common, J. E. A.; Ogg, S. C.; Chen, H.; Sim, S. Y.; Goh, W. L. R.; Ng, K. W.; Simpson, J. A.; Chee, L. L.; Eng, G. H.; Li, B.; Lunny, D. P.; Chuon, D.; Venkatesh, A.; Khoo, K. H.; Mclean, W. H. I.; Lim, Y. P.; Lane, E. B. The human intermediate filament database: Comprehensive information on a gene family involved in many human diseases. *Hum. Mutat.* **2008**, *29*, 351–360.
- (48) Bjelkmar, P.; Larsson, P.; Cuendet, M. A.; Hess, B.; Lindahl, E. Implementation of the CHARMM Force Field in GROMACS: Analysis of Protein Stability Effects from Correction Maps, Virtual Interaction Sites, and Water Models. *J. Comput. Chem.* **2010**, *6*, 459–466.
- (49) Jorgensen, W. L.; Chandrasekhar, J.; Madura, J. D.; Impey, R. W.; Klein, M. L. Comparison of simple potential functions for simulating liquid water. *J. Chem. Phys.* **1983**, *79*, 926–935.
- (50) Hess, B.; Bekker, H.; Berendsen, H. J. C.; Fraaije, J. G. E. M. LINCS: A linear constraint solver for molecular simulations. *J. Comput. Chem.* **1997**, *18*, 1463–1472.
- (51) Darden, T.; York, D.; Pedersen, L. Particle Mesh Ewald—An $N \log(N)$ Method for Ewald Sums in Large Systems. *J. Chem. Phys.* **1993**, *98*, 10089–10092.
- (52) Essmann, U.; Perera, L.; Berkowitz, M. L.; Darden, T.; Lee, H.; Pedersen, L. G. A Smooth Particle Mesh Ewald Method. *J. Chem. Phys.* **1995**, *103*, 8577–8593.
- (53) Bussi, G.; Donadio, D.; Parrinello, M. Canonical sampling through velocity rescaling. *J. Chem. Phys.* **2007**, *126*, 014101.
- (54) Parrinello, M.; Rahman, A. *Phys. Rev. Lett.* **1980**, *45*, 1196–1199.
- (55) Cistola, D. P.; Hamilton, J. A.; Jackson, D.; Small, D. M. Ionization and Phase-Behavior of Fatty-Acids in Water—Application of the Gibbs Phase Rule. *Biochemistry (Moscow)* **1988**, *27*, 1881–1888.
- (56) Kim, H.; Choi, Y.; Kim, J. I.; Jeong, K.; Jung, S. Molecular Modeling Studies on the Chiral Separation of (\pm)-Catechins by Mono-succinyl-beta-cyclodextrin. *Bull. Korean Chem. Soc.* **2009**, *30*, 1373–1375.
- (57) Eisenhaber, F.; Lijnzaad, P.; Argos, P.; Sander, C.; Scharf, M. The Double Cubic Lattice Method—Efficient Approaches to Numerical-Integration of Surface-Area and Volume and to Dot Surface Contouring of Molecular Assemblies. *J. Comput. Chem.* **1995**, *16*, 273–284.
- (58) Kumar, S.; Bouzida, D.; Swendsen, R. H.; Kollman, P. A.; Rosenberg, J. M. The Weighted Histogram Analysis Method for Free-Energy Calculations on Biomolecules. *J. Comput. Chem.* **1992**, *13*, 1011–1021.
- (59) Donlon, L.; Nordin, D.; Frankel, D. Complete unfolding of fibronectin reveals surface interactions. *Soft Matter.* **2012**, *8*, 9933–9940.
- (60) Hane, F. T.; Atwood, S. J.; Leonenko, Z. Comparison of three competing dynamic force spectroscopy models to study binding forces of amyloid-B (1–42). *Soft Matter.* **2014**, *10*, 1924–1930.
- (61) Lee, C. K.; Wang, Y. M.; Huang, L. S.; Lin, S. Atomic force microscopy: Determination of unbinding force, off rate and energy barrier for protein–ligand interaction. *Micron* **2007**, *38*, 446–461.
- (62) Schwesinger, F.; Ros, R.; Strunz, T.; Anselmetti, D.; Güntherodt, H. J.; Honegger, A.; Jermutus, L.; Tiefenauer, L.; Plückthun, A. Unbinding forces of single antibody–antigen complexes

correlate with their thermal dissociation rates. *Proc. Natl. Acad. Sci. U. S. A.* **2000**, *97*, 9972–9977.

(63) Sulcek, T. A.; Friddle, R. W.; Langry, K.; Lau, E. Y.; Albrecht, H.; Ratto, T. V.; DeNardo, S. J.; Colvin, M. E.; Noy, A. Dynamic force spectroscopy of parallel individual Mucin 1–antibody bonds. *Proc. Natl. Acad. Sci. U. S. A.* **2005**, *102*, 16638–16643.

(64) Barbana, C.; Perez, M. D.; Sanchez, L.; Dalgalarondo, M.; Chobert, J. M.; Haertle, T. Interaction of bovine alpha-lactalbumin with fatty acids as determined by partition equilibrium and fluorescence spectroscopy. *Int. Dairy J.* **2006**, *16*, 18–25.

(65) Balendiran, G. K.; Schnutgen, F.; Scapin, G.; Borchers, T.; Xhong, N.; Lim, K.; Godbout, R.; Spener, F.; Sacchettini, J. C. Crystal structure and thermodynamic analysis of human brain fatty acid-binding protein. *J. Biol. Chem.* **2000**, *275*, 27045–27054.

(66) Frazier, R. A.; Papadopoulou, A.; Green, R. J. Isothermal titration calorimetry study of epicatechin binding to serum albumin. *J. Pharm. Biomed. Anal.* **2006**, *41*, 1602–1605.

(67) Lacal, J.; Alfonso, C.; Liu, X. X.; Parales, R. E.; Morel, B.; Conejero-Lara, F.; Rivas, G.; Duque, E.; Ramos, J. L.; Krell, T. Identification of a Chemoreceptor for Tricarboxylic Acid Cycle Intermediates: Differential chemotactic response towards receptor ligands. *J. Biol. Chem.* **2010**, *285*, 23124–23134.